PHILOSOPHICAL TRANSACTIONS OF THE ROYAL SOCIETY A MATHEMATICAL, PHYSICAL & ENGINEERING SCIENCES

Aspects of Chemical Shift Imaging which Illustrate the Cross-Fertilization of Methods and Techniques in in vivo NMR Imaging and Spectroscopy [and Discussion]

C. J. Baudouin, D. J. Bryant, A. G. Collins, G. C. Coutts, I. J. Cox, J. V. Hajnal, D. K. Menon, D. R. Page, I. R. Young and R. D. Farrant

Phil. Trans. R. Soc. Lond. A 1990 **333**, 545-559
doi: 10.1098/rsta.1990.0182

Aspects of chemical shift imaging which illustrate the cross-fertilization of methods and techniques in *in vivo* NMR imaging and spectroscopy

By C. J. Baudouin[1], D. J. Bryant[1], A. G. Collins[1], G. C. Coutts[1], I. J. Cox[1], J. V. Hajnal[1], D. K. Menon[1], D. R. Page[2] and I. R. Young[1]

[1]*NMR Unit, Hammersmith Hospital, DuCane Road, London W12 0HS, U.K.*
[2]*IBM Research Laboratory, Winchester, Hants, U.K.*

We discuss the methods of chemical shift imaging, or distributed NMR spectroscopy using techniques derived from NMR imaging. We point out that the problems, and artefacts, of most localized spectroscopy are substantially those of imaging, and that lessons learnt from the latter, and strategies developed for it, can be used to improve the quality of spectral data in many ways. Perhaps just as important now are the techniques used in spectroscopy which are being imported into imaging to provide additional contrast mechanisms, and, hopefully, data about tissue which cannot be obtained using other methods.

1. Introduction

In vivo nuclear magnetic resonance spectroscopy (MRS) and imaging (MRI) are thought of by many as being quite distinct topics, even if the physical processes underlying both, and the equipment on which the experiments are performed, are identical. This distinction lies in the very different forms of the results presented, and in the way in which these are subsequently analysed. It is the purpose of this paper to demonstrate how interdependent the methods actually are.

A major area of overlap is known as chemical shift imaging (CSI), which, to spectroscopists, implies the extraction of spectral data from a large array of contiguous voxels using gradient pulse encoding, and, to imagers, the production of images wherein components with different chemical shifts are displayed, or otherwise differentiated, separately. In the latter case, normally, it means the separation of lipid- and water-based signals.

The first section of the paper is a brief summary of the strategies used to obtain the data in their traditional form. The second is an outline of the ways in which spectroscopic studies can be influenced and improved by the use of data obtained from imaging experiments. The third gives examples of the way in which techniques developed for spectroscopic purposes can be productively applied to obtain more informative images.

2. Chemical shift imaging methods

The basic chemical shift imaging experiment in spectroscopy is that first proposed by Brown *et al.* (1982). In this method, one or more short position encoding gradient pulses are applied to the system immediately after excitation of the magnetization

Figure 1

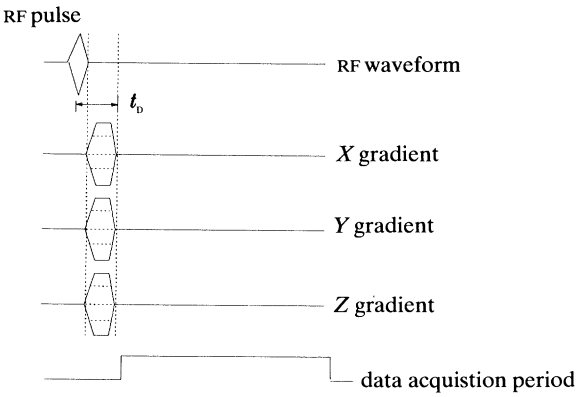

Figure 2

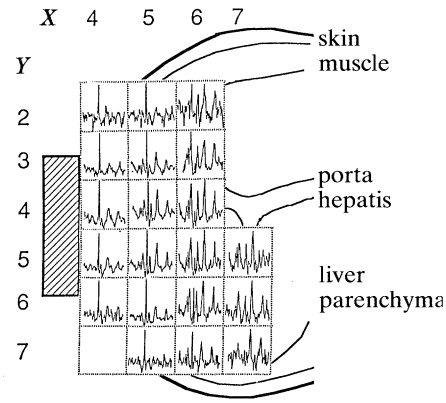

Figure 1. Diagram of the sequence timing for a four-dimensional acquisition of data from, for example, an *in vivo* ^{31}P study. The dashed appearance of the X, Y, Z gradient pulses indicate their variation one experiment to another, in one complete acquisition all permutations of amplitude are used. (Thus if the matrix of individual voxels is specified to be $n \times n \times n$ then each gradient has n values during the experiment, and a total of n^3 acquisitions is the minimum permissible.)

Figure 2. Section of a plane of 64 spectra (8×8) from a four-dimensional data-set with a matrix of $8 \times 8 \times 8$ (512 spectra). A total of 1024 acquisitions were used (to allow for phase alternation of the RF pulse to minimize DC level offset effects (Hoult & Richards 1975) with a repetition time of 1 s, meaning that acquisition took around 18 min. The data were cosine filtered in all three spatial directions. Note the rolling baseline artefact characteristic of the loss of the early data points lost during the phase encoding interval (t_D in figure 1). Spatial resolution was a nominal 20 mm^3. Row and column numbers are marked, and the location of the detector coil is shown shaded.

to lie in the X–Y plane, and data are recovered thereafter in the absence of any further gradient field operation (as is illustrated in figure 1). The method has been most extensively exploited *in vivo* for the acquisition of phosphorus 31 spectra (Bailes *et al.* 1988), for which spatial resolution matrices of up to $14 \times 14 \times 10$ have been obtained (Weiner 1990).

Since, as noted in the legend of figure 1, all combinations of the gradient are needed to define a data-set, with data acquisition times of not less than 45 min being needed, many acquisitions are recovered using encoding in only one spatial dimension (Bailes *et al.* 1987) with localization in the other directions being determined by the configuration of signal detector used (most often a small surface coil (Ackerman *et al.* 1980)). This method is frequently used in conjunction with other localization methods, particularly for proton spectroscopy (Luyten *et al.* 1988; Young *et al.* 1989).

Figure 2 is part of a plane of data from a four-dimensional acquisition of phosphorus 31 signals from the liver of a patient. Some of the features of such sets of spectra will be discussed later as part of the analysis of ways in which cross-fertilization can be demonstrated. The individual peaks from a data-set such as that in figure 2 can be extracted and used as the basis of a set of metabolite maps, though these are invariably of low resolution, and much spatial filtering is used to make them into acceptable images.

Chemical shift imaging in the other sense depends on mapping the two components (lipid and aqueous) that appear in proton data-sets to a sufficient degree to allow for a simple and direct extension of standard imaging procedures in an acceptable time. All the methods exploit phase differences arising between the two components with

PHILOSOPHICAL TRANSACTIONS OF THE ROYAL SOCIETY A MATHEMATICAL, PHYSICAL & ENGINEERING SCIENCES

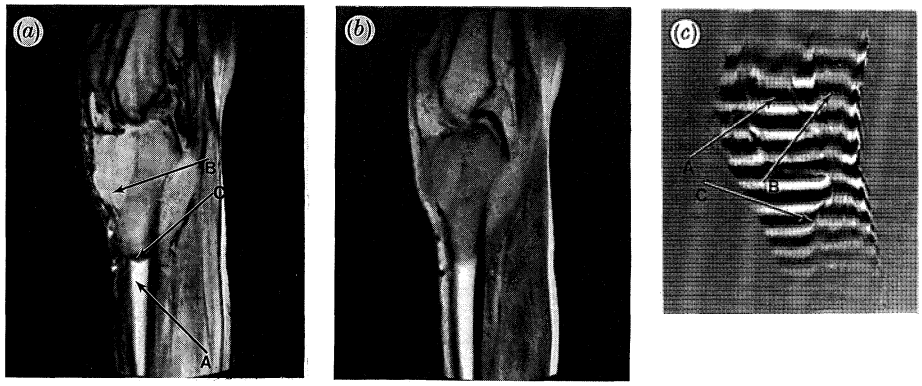

Figure 3. Illustration of the manipulation of image contrast and data through the use of methods dependent on the chemical shift difference between water and lipid components of an image. (*a*) Magnitude image acquired with T_E chosen to give a phase difference of π between the two components ($T_E = 22$ ms, at a field of 0.15 T). The image is of a patient with an osteosarcoma; the magnitude of the signal from the fat components in the bone marrow (arrow A) is similar to that from the tumour (arrow B). The line (arrow C) between the two is the place where the signals from the two overlap in the same voxels, and cancel, because they are out of phase, so that a minimum is observed. (*b*) Hahn spin echo of the same patient, with no dephasing between the lipid and water components, and, consequently, loss of the delineating line seen in figure 3*a*. (*c*) 'Zebra stripe' image of the leg of a volunteer in which a phase difference imposed by the phase correction of one image by another (see main text) results in a phase pattern, which is shifted between the lipid and water components (arrows A, B). The image also shows the characteristic distortion of phase lines due to moving spins (in the blood vessels, for example) (arrow C, and see main text).

their approximate 3.5 p.p.m. chemical shift. The typical method is that of Dixon (1984) in which, in principle, two images are acquired, with their data acquisitions symmetrically displaced from being centrally located at a Hahn spin echo (Hahn 1950) by a time t_s given by

$$t_s = \pi/4\gamma B_0 \delta, \tag{1}$$

where γ is the gyromagnetic ratio; B_0 the main field and δ the chemical shift between the species. Variations of this basic observation have been exploited in a variety of ways, two of which are illustrated in figure 3.

The first image (figure 3*a*) is a magnitude reconstruction of a gradient recalled echo image (Hutchison *et al.* 1980) in which the period T_E (using a variant of the American College of Radiology notation (1983)) from excitation to the echo formed by refocusing the magnetization is given by (cf. equation (1)):

$$\pi = \gamma T_E B_0 \delta \tag{2}$$

at which time the lipid and water component signals are out of phase. (Figure 4 is a diagram of the sequences used in obtaining images such as those in figure 3*a* and *c*.) The second image (figure 3*b*) is a conventional Hahn echo image of the same patient as in figure 3*a*. In the former image, the intensity of the signals from the bone marrow (arrow A) and tumour (arrow B) are not dissimilar, but the signals are out of phase, as seen by the delineation marked by arrow C, where there is a loss of net intensity where signals from the two components overlap in the same voxel, and mutual cancellation occurs (Bydder & Young 1985*a*).

Figure 3*c* shows another, more complex, use of phase to characterize and explore chemical shift and other phase differences. The image is created from two data-sets,

PHILOSOPHICAL TRANSACTIONS OF THE ROYAL SOCIETY A MATHEMATICAL, PHYSICAL & ENGINEERING SCIENCES

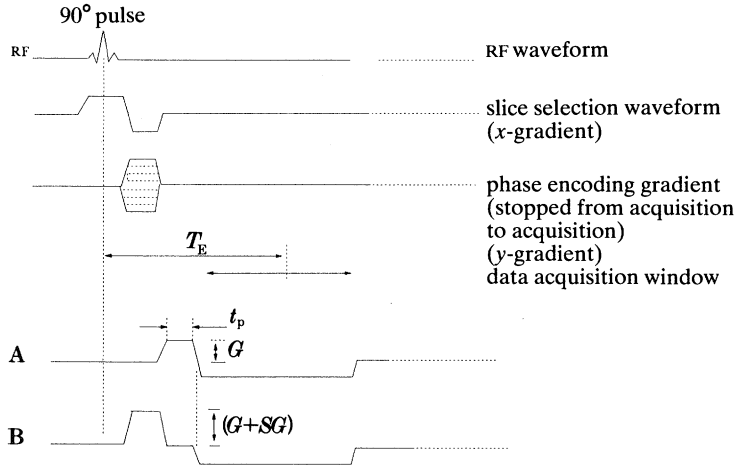

Figure 4. Sequence diagram to show the procedures used to form the images in figure 3*a* and *c*. The two different data acquisition gradients used to produce the feature in figure 3*c* are marked A and B. A was used as phase reference for the real reconstruction of B. t_p is the effective pulse duration (as though the pulse was square).

in one of which a phase offset was introduced relative to the other by a small relative adjustment of the amplitude of the offsetting gradient pulse used to allow the formation of an echo at around the centre of the data acquisition interval. This means that similar data points taken of the signals in the two acquisitions reflect a phase offset the magnitude of which is given by $\gamma\delta G t_p$ where δG is the difference between amplitudes of the two 'warping' gradients (Hutchison *et al.* 1980) and t_p is the effective duration of the pulse. If the matrix size in the data acquisition is n, and the magnitude of the warping gradient used to form the one of the two data acquisitions to be used as reference, as will be described, is G, then the number of stripes (δn) across the image field is given by:

$$\delta n/n = \delta G/G. \tag{3}$$

The effect (described as a 'zebra stripe' image by its first users (Wedeen *et al.* 1986)) results when the second image is reconstructed as a real image, with any phase variations due to machine artefacts, or other effects, being corrected by assuming they introduce similar changes in the first (reference) image. The deliberate offset in phase between the two data-sets is reflected in the image shown.

For the purposes of the paper, however, the feature of the image which is of interest is the offset in phase between the lipid and water components (arrows A and B) reflected across the whole image.

Another phase effect has also been deliberately introduced into the image: by offsetting the timing of one of the warping pulses relative to the other as shown in figure 4 (Nayler *et al.* 1986). This results in the introduction of a further phase difference (φ_v) into spins which are moving given by

$$\varphi_v = \gamma v t_p t_D (G + \delta G), \tag{4}$$

where t_D is the relative displacement of the two pulses, and v is the velocity of motion of the spins in the direction of flow sensitization. Any macroscopic motion results in distortion of the phase bars as shown by arrow C.

3. The relevance of imaging concepts to spectroscopic studies

It is assumed to be desirable to have imaging data to assist in the determination of the locations from which spectral data is to be recovered. It is less well appreciated that the arguments used by Brunner & Ernst (1979) in imaging that there is no loss of signal-to-noise ratio during the use of phase encoding techniques are applicable so that, if data must be averaged to obtain adequate quality from a specified volume, it is preferable to encode it spatially at the same time, to cover many voxels in parallel.

Figure 5 illustrates the value of this strategy. It shows an abnormal proton spectrum acquired from the brain of a patient suffering from AIDS compared with that from a normal control. The technique used selection of a region by the MESA method (Lampman *et al.* 1986) with water suppression by a $1\bar{3}3\bar{1}$ binomial pulse sequence (Hore 1983), followed by further phase encoding in one dimension. The importance of the result is that the spectrum was derived from part of the brain which was normal on other studies (MRI and X-ray computerized tomography (Hounsfield 1973)) though its abnormality better reflected known neurological deficit than they did. Since biological variation is so great, the opportunity to compare normal and abnormal regions can only be discarded with caution (Cox *et al.* 1988).

A feature from localization is that there is often less reduction in the signal-to-noise ratio than might be expected as the volume from which signal is obtained is reduced in circumstances where the data acquisition bandwidth is constant. This is because voxel field homogeneity may be so far improved that T_2^* (the effective spin–spin relaxation time constant) approaches more closely to T_2. (T_2^* is related to T_2 via the relation (Abragam 1961)

$$1/T_2^* = 1/T_2 + \gamma \delta B_0, \tag{5}$$

where δB_0 is the field deviation throughout the volume from which signal is detected.) The signal-to-noise ratio in most spectral acquisitions is a function of $(T_2^*)^{\frac{1}{2}}$.

Figure 6 illustrates what is observed. The data are all proton spectra acquired as in the previous example with T_E 270 ms, and T_R 2 s, from a patient with chronic renal failure. The left-hand spectrum is from a whole selected volume, the set of eight on the right are the result of one-dimensional phase encoding of the volume, and show much less loss of signal-to-noise ratio than would be expected, as the number of data acquisitions in the two experiments were respectively 128 (left-hand spectrum) and 256 (phase encoded spectra).

However, localization can result in additional, or substantially different, artefacts from those normally encountered in spectroscopy, and this section continues with some applications of imaging concepts to improve spectroscopic studies in other ways. These fall into two groups: (*a*) mapping of both DC and RF fields to predict the actual performance of, and possible corrections for, localized spectroscopy; (*b*) applying the body of knowledge about the formation and content of artefacts in imaging to improve the performance of spatial encoded spectroscopy.

Both topics have been reviewed fairly extensively recently in the literature (Young *et al.* 1989*b*) and we propose only to mention points covered in that paper briefly, though we discuss other aspects more fully.

PHILOSOPHICAL TRANSACTIONS OF THE ROYAL SOCIETY A MATHEMATICAL, PHYSICAL & ENGINEERING SCIENCES

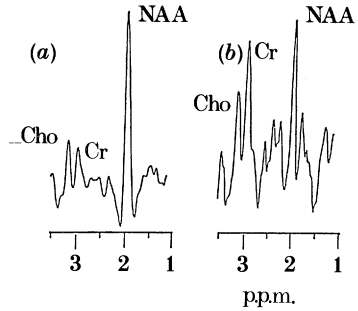

Figure 5. Proton spectrum from (*a*) the brain of an AIDS patient, as described in the text, shown adjacent to that (*b*) from a normal control. Slices were approximately $40 \times 40 \times 5$ mm in size in these studies. The *n*-acetyl aspartate (NAA) peak in the patient study is substantially smaller relative to either the creatine or choline peaks than in a normal spectrum.

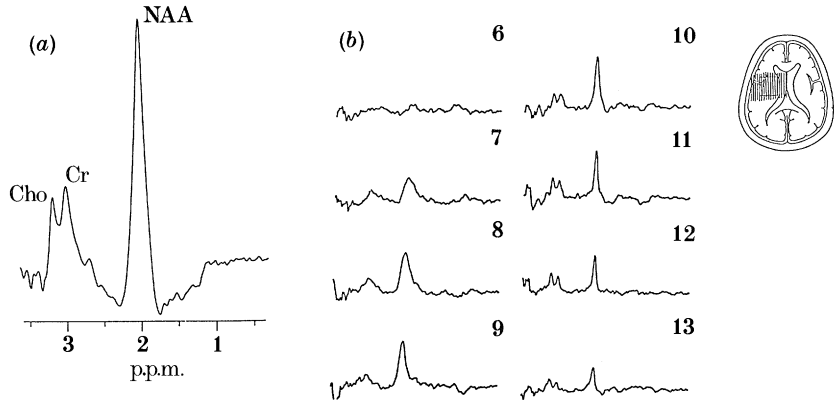

Figure 6. Proton spectra from the brain of a patient with chronic renal failure. The left-hand single spectrum (*a*) was from a volume of 40 mm^3, otherwise not resolved. Water suppression was by $\bar{1}33\bar{1}$ bionomial pulse pattern (Hore 1983). The right-hand set of eight spectra (*b*) were the result of phase encoding the same volume in one direction (as shown in the small inset diagram). Quantifying apparent relative improvement in signal-to-noise ratio is not useful since the improvements obtained with localization are artefacts of individual experiments. Only twice the number of data recoveries were used in the localized case.

3.1. *Main field mapping*

The obvious motivation for mapping the field in a region from which spectra are to be recovered is that the knowledge may allow field inhomogeneity to be improved by better shimming. The more subtle, and less well understood, reason is to determine the impact of local susceptibility variations due to the body itself, which are found both in normal structures and in diseased tissue. This is of particular relevance since haemorrhagic deposits are associated with a great many lesions apart from the immediately obvious incidence of a significant bleed. For example, it has been reported using the delayed gradient recalled echo methods developed by Cox *et al.* (1986) that susceptibility variations of greater than 0.2 p.p.m. occur in around 50 % of adult brain tumours (Collins *et al.* 1988). The major source of effects due to blood are the degradation products of haemoglobin, which exhibit varying degrees of paramagnetism (Bradley 1988) and, it has been suggested (Koenig *et al.* 1986), even superparamagnetism, or ferromagnetism.

The exploitation of the data to try and improve spectral quality is another promising avenue. A perception of the possibility is illustrated in figure 7, which shows, in figure 7*a*, the image of a plane and in figure 7*b* its phase map, the one-dimensional spatially encoded spectrum from which is shown in figure 7*c*. This is the signal from an aqueous phantom and should have the classic lorentzian line shape. Instead it bears a marked resemblance to the histogram of field distribution (figure 7*d*, voxel resonant frequency along the abscissa; number of voxels along the ordinate) derived from the map in figure 7*b*. This suggests that the data in figure 7*d* could be used to correct the result in figure 7*c*.

Processing in the time domain has so far proved unsatisfactory and we are currently using maximum entropy processing (Laue *et al.* 1985) to evaluate the relationship $R = FS$ (where R is the observed spectrum, S the true spectrum and F is the field inhomogeneity distribution, equivalent to the point spread function) using the relations (Page *et al.* 1990):

$$A_1 = R, \quad A_{n+1} = kA_n \exp\{RF^{\mathrm{M}}/(A_n^* F + 1) - 1\}, \tag{6}$$

where A_{n+1} is the result of the nth iteration, and, F^{M} is the mirror of F. The process is run until either the error deviation (the root mean square of $R/(A_n F + 1)$) starts to increase again, or until 20 passes are completed. Figure 7*e* illustrates the outcome of processing figure 7*c*, and is typical of early results.

3.2. *Assessment of* RF *homogeneity*

Accurate knowledge of the local RF field intensity also is essential where quantitation is to be attempted. Many strategies have been proposed for RF mapping (Hoult & Chen 1988; Perman *et al.* 1989), and for designing procedures which avoid artefacts from the use of, for example, the highly nonlinear field profiles produced by surface coils (Ackerman *et al.* 1980), and are comprehensively described elsewhere.

3.3. *Region formation artefacts*

These are a problem directly analogous to the slice formation artefacts (Young *et al.* 1985; Foster 1985) that affect imaging; and arise with any localization technique involving selective excitation (Garroway *et al.* 1974) using gradient fields. In the chemical shift imaging experiments, the problems arise when a large region is formed selectively, before phase encoding. The problem occurs potentially when the repetition time (T_{R}) of a selective experiment is not much longer than T_1, and becomes worse as T_{R} is reduced towards T_2.

3.4. *Motion artefact effects*

All imaging specialists are immediately aware of the impact on their work of motion artefacts, which appear as variably intense 'ghosts' of the proper image lying across the data, and largely invalidate efforts to quantify images accurately, and even degrade them to the point where diagnostic performance is totally lost. Magnetic resonance imaging of the abdomen is regarded as being very much harder and less satisfactory than that of the brain for this reason. As has been demonstrated elsewhere (Young *et al.* 1989*b*) the impact of motion on localized spectra is not immediately obvious, and, more often than not, the only symptom is an unexpectedly poor signal-to-noise ratio for the experiment performed. Variability in the quality of results for no apparent reason is another symptom. However, a realistic approach assumes motion artefacts in any results from the heart or abdomen.

PHILOSOPHICAL TRANSACTIONS OF THE ROYAL SOCIETY A MATHEMATICAL, PHYSICAL & ENGINEERING SCIENCES

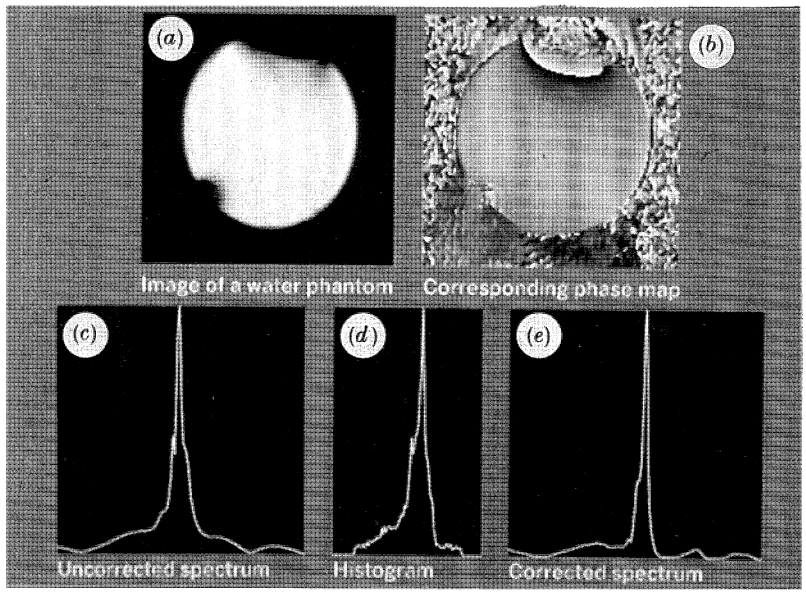

Figure 7. Illustration of the similarity between the line shape of a simple spectrum and histograms formed from the voxel field deviations as observed through field mapping, and the use of the latter for line-shape correction. (*a*), (*b*) Magnitude image and phase map of a plane from which one spectrum in a one-dimensional phase encoding ^{1}H spectroscopic experiment is to be recovered. (*c*) Spectrum extracted from the plane in (*a*). (*d*) Histogram of the field deviations mapped in image (*b*). Note the similarity of the shape of (*c*) and (*d*), though the former should be a lorentzian. (*e*) Corrected spectrum formed as described in the text.

3.5. *Time constant effects*

Though relaxation time constants have long had to be considered as possible parameters in spectroscopy, their impact in *in vivo* work is much greater. Many metabolite time constants are very long, and repetition times of 15 s have been used in an attempt to avoid unpredictable saturation effects (Naruse *et al.* 1989). If significant localization is sought the times needed to acquire data can become intolerable.

An additional complication is that it is not sufficient to interpolate time constants from one study, or model system, to another. Thus, metabolite time constants vary from one tissue to another, and can often seem to vary quite dramatically from normal to abnormal tissue. Although this could be a true variation, as is found in water in imaging studies, it is normally assumed to be due to the presence of overlapping peaks of metabolites present in different relative concentrations between normal and abnormal tissues. This is frequently observed in the phosphorus monoester (PME) and phosphorus diester (PDE) regions of the phosphorus spectrum in liver pathology (Cox *et al.* 1988). In these regions there are multiple very close peaks (Bell *et al.* 1989) only so far partly resolved particularly by proton decoupling (Luyten *et al.* 1989), but more often than not unresolved.

Figure 8 shows two sets of spectra of the liver, the left-hand set of a volunteer, the right of a patient with hepatitis. Both sets are individual spectra from one-dimensionally localized experiments, taken at identical patterns of repetition time. The differences in the PME and PDE regions are marked, with the apparent time constant of the former increasing in the patient, while that of the latter decreases (a

PHILOSOPHICAL TRANSACTIONS OF THE ROYAL SOCIETY A MATHEMATICAL, PHYSICAL & ENGINEERING SCIENCES

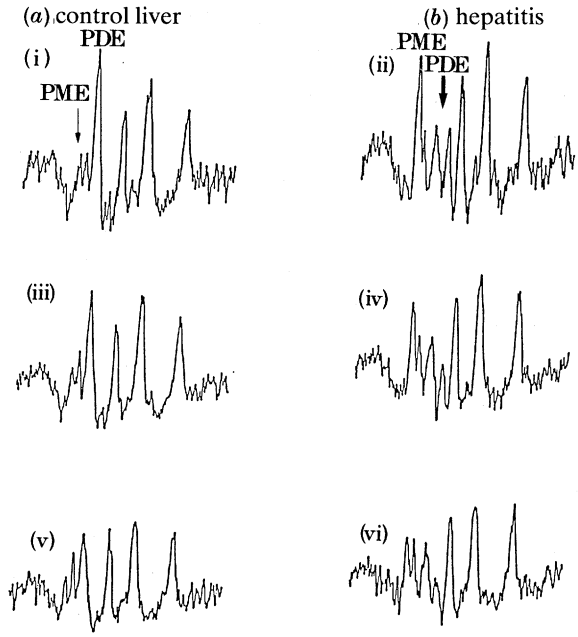

Figure 8. Two sets of one-dimensional spectra from a volunteer (column 1) and patient (column 2), at identical patterns of T_R to show differences in the relative time constant of the PME and PDE peaks (bottom to top lines, respectively: $T_R = 0.5$ s, 1.0 s, 5.0 s).

reasonably common observation in liver disease). Resolution of the components in such peaks is complicated by shimming problems, including those due to susceptibility, and by possible problems of exceeding acceptable RF doses (National Radiological Protection Board 1983) inhibiting the use of proton decoupling. In general, it can be assumed that it will not be possible to achieve adequate resolution to separate the component peaks reliably. Methods derived from efforts to separate components of different relaxation time constants in imaging (Brosnan *et al.* 1988) may prove to be a route forward.

4. The use of spectroscopic techniques in imaging studies

The early techniques used in imaging were aimed almost entirely at developing image contrast derived from deviations in the time constants of normal and abnormal tissue, together with a steady improvement in the speed with which patient examinations could be completed. Later attention switched towards the monitoring, particularly, of flow but, also, of physiological parameters. Only latterly have significant efforts been made to apply spectroscopic techniques to imaging.

4.1. *Use of solvent suppression techniques in imaging*

As is now emerging there are a number of areas of clinical imaging practice where the selective excitation of either the water or fat lines of the sample whole body spectrum is proving useful. These include instances where it is desired to observe the effects of contrast material such as Gadolinium diethylpentacetic acid (Gd-DTPA) (Weinman *et al.* 1984) in regions of the body where there are heavy fatty deposits. Since the practical consequence of Gd-DTPA is, at lower concentrations, a reduction

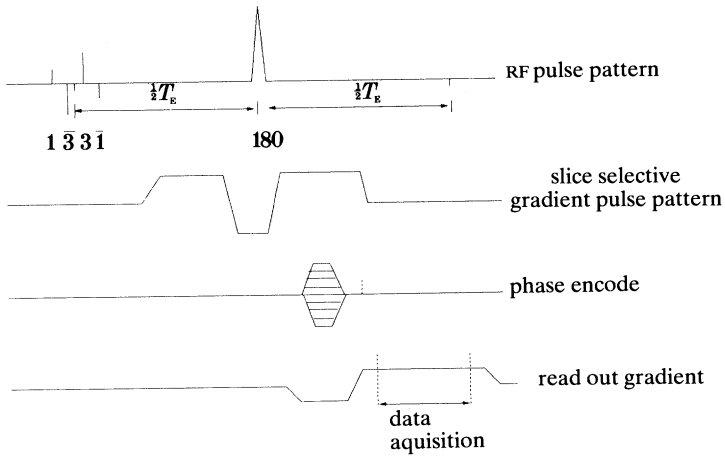

Figure 9. Sequence diagram for a chemically selective imaging experiment. Selection of fat or water components is determined by the actual carrier frequency used for the $1\bar{3}3\bar{1}$ pulse pattern. The RF pulse frequency in the presence of the gradient is not, in effect, chemically selective, but the frequency used determines the place at which selective inversion is performed, and the slice obtained is formed. (Actually, chemical shift effects mean that two not quite overlapping slices are generated (one for fat, the other water) but as long as the selective gradient used is adequately large the shift is unimportant.) The large 'spoiling' gradient pulses on either side of the slice selective gradient help eliminate unwanted signals.

of T_1, generally this causes the appearance of places where it lodges to become more like that of fat (which is, typically, amongst the brightest part of an image). It is thus easier to detect what is happening in the absence of the fat signal. Because of its dependency on T_1 the principle method clinically used for eliminating fat signals (Bydder & Young 1985*b*) is then inappropriate.

The methods used involve selectively exciting only the water signals using binary RF pulse patterns as described by Hore (1983) and originally applied in high-resolution spectroscopy for solvent suppression. Though the original application of the method was in susceptibility mapping (Hall *et al.* 1989), it has proved substantially more effective in resolving the problem outlined above (Chacko *et al.* 1989). Figure 10 shows the effectiveness of the technique even at the low field of 0.15 T where evolution times between the RF pulses of the selective pattern are very long. The figure shows the normal spin-echo image of the calf of a volunteer (figure 10*a*), side by side with the selectively excited water image (figure 10*b*).

4.2. *Magnetization transfer studies*

Another major application of a spectroscopic concept has emerged in imaging recently (Wolff & Balaban 1989), and its impact is as yet impossible to assess. This is the use of very long off-resonance RF pulses applied before other, relatively standard, imaging procedures intended to show magnetization transfer between the large molecules of the cellular structures (signals from which are invisible in standard imaging studies), and the free water pool that is monitored. The complications arise from the diversity of effects which are involved, the resolution of which, when satisfactorily accomplished, is necessarily going to be time consuming, so contradicting the imperative in patient examinations that the study be swift.

Experiments involving prolonged RF excitation in imaging which have been

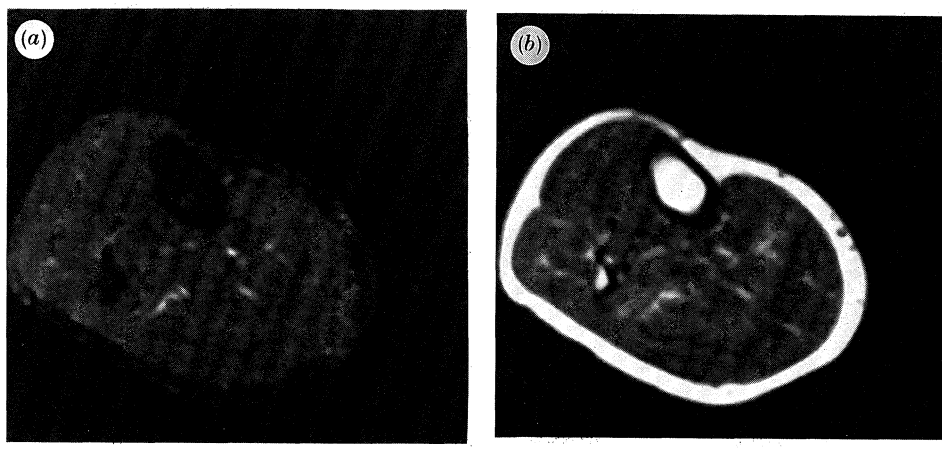

Figure 10. Images to illustrate the use of the selective excitation method described. Both images have a matrix of 128×128; slice thickness of 10 mm; resolution of 1.5 mm^2, and sequence repetition time 1500 ms. (*a*) Normal spin echo. (*b*) Image in which only the water line has been excited.

reported include studies of T_1 in the rotating frame (Sepponen *et al.* 1985; Young 1988; Santyr *et al.* 1989), pseudo-magic-angle spinning (De Luca *et al.* 1986; Zhong *et al.* 1990) as well as the magnetization transfer, or cross relaxation, mentioned above. The saturation effects noted by Henkelman (1990) are also involved, and multiple experiments are needed to elucidate the effects, each of which may take several minutes.

As a very brief illustration we use some of our own recent results. Firstly, table 1 displays the ratio of the calculated values of T_2 (from pairs of observations at different T_E) with and without irradiation at different frequency offsets for human calf muscle (the average value of five small regions from each of two very preliminary studies):

offset frequencies	500 Hz	814 Hz	1 kHz	2 kHz	5 kHz	10 kHz
$\frac{T_2 \text{ with}}{T_2 \text{ without}}$	2.03	2.30	1.95	1.35	1.14	0.98

The predicted maximum line narrowing would occur at 814 Hz with the experimental parameters used.

In the second example, figure 11 shows a pair of images obtained with the parameters stated in the legend, contrasting one with irradiation (figure 11*b*) with one without (figure 11*a*). The differences in the images are very apparent and, at one level, it is quite possible for radiologists to accept the process as one potentially generating additional image contrast, without being aware why changes occur.

The *in vivo* experimental problem in resolving what contributions are arising from which mechanism is determined ultimately by the need to avoid the delivery of RF doses to the patient, which exceed safety guidelines (NRPB 1983).

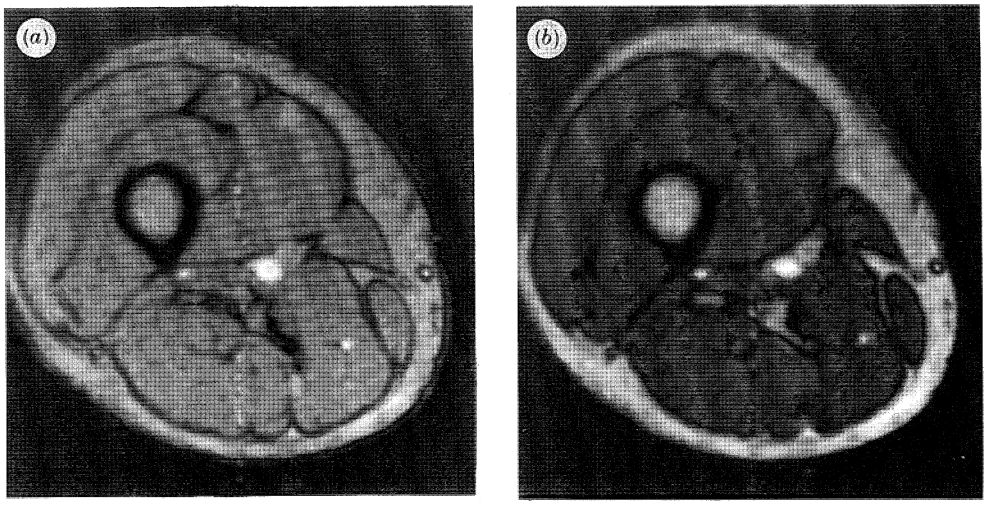

Figure 11. Pair of images obtained with $T_R = 1000$ ms, $T_E = 44$ ms; matrix 128×128; resolution 1.5×1.5 mm; slice thickness 10 mm. (*a*) Normal spin echo. (*b*) Same acquisition as above except with 100 ms RF pre-pulse of 27 μT irradiation at an offset frequency of 2 kHz from resonance.

5. Conclusions

Though the developments of *in vivo* magnetic resonance imaging and spectroscopy, for a significant part of their existence, have seemed remote from each other, it is apparent that, in the concepts and practice of chemical shift imaging they have now largely coalesced. It is likely that, if accurate quantitation and measurement is the target in either, methods and ideas derived from the other are almost essential. In *in vivo* studies, particularly of patients, it is wisest to assume that there will be an adequate period to get only a small part of the data which are desirable, and to structure and examination so that data with some, if limited, value are acquired from the very start, then build on that. This, more than anything else, provides a limitation on quantification which may never be completely avoided.

We thank the Medical Research Council for their continuing help and support during the clinical investigations of *in vivo* magnetic resonance which we have been undertaking, and our other colleagues who have supported us so well during our studies.

References

Abragam, A. 1961 *The principles of nuclear magnetism*, p. 50 *et seq.* Oxford: Clarendon Press.

Ackerman, J. J. H., Grove, I. H., Wong, G. C., Gadian, D. G. & Radda, G. K. 1980 Mapping of metabolites in whole animals by 31P using surface coils. *Nature, Lond.* **283**, 167.

American College of Radiology Glossary of NMR Terms 1983 Chicago: ACR.

Bailes, D. R., Bryant, D. J., Bydder, G. M., Case, H. A., Collins, A. G., Cox, I. J., Evans, P. E., Harman, R. R., Hall, A. S., Khenia, S., McArthur, P., Oliver, A., Rose, M. R., Ross, B. D. & Young, I. R. 1987 Localized phosphorus-31 NMR spectroscopy of normal and pathological human organs *in vivo* using phase-encoding techniques. *J. magn. Reson.* **74**, 158–170.

Bailes, D. R., Bryant, D. J., Case, H. A., Collins, A. G., Cox, I. J., Hall, A. S., Harman, R. R., Khenia, S., McArthur, P., Ross, B. D. & Young, I. R. 1988 *In vivo* implementation of three dimensional phase encoded spectroscopy with a correction for field inhomogeneity. *J. magn. Reson.* **77**, 460–470.

Bell, J. D., Cox, I. J., Sargentoni, J., Peden, C. J., Menon, D. K., Bryant, D. J., Coutts, G. A., Iles,

PHILOSOPHICAL TRANSACTIONS OF THE ROYAL SOCIETY A MATHEMATICAL, PHYSICAL & ENGINEERING SCIENCES

R. A., Gadian, D. G. & Young, I. R. 1989 *In-vivo* and *in-vitro* MRS Study of the PME and PDE peaks in human liver. *Proc. 8th A. Mtg Soc. Magn. Reson. Med., Amsterdam*, p. 1053.

Bradley, W. G. 1988 MRI of hemorrhage and iron in the brain. In *Magnetic resonance imaging* (ed. D. D. Stark & W. G. Bradley), pp. 359–374. St Louis: Mosby.

Brosnan, T., Wright, G., Nishmura, D., Cao, Q., Macovski, A. & Sommer, F. G. 1988 Noise reduction in magnetic resonance imaging. *J. magn. Reson.* **8**, 384–498.

Brown, T. R., Kincaid, B. M. & Ugurbil, K. 1982 NMR chemical shift imaging in three dimensions. *Proc. natn. Acad. Sci. U.S.A.* **79**, 3523.

Brunner, P. & Ernst, R. R. 1979 Sensitivity and performance time in NMR imaging. *J. magn. Reson.* **33**, 81.

Bydder, G. M. & Young, I. R. 1985*a* Clinical use of the partial saturation and saturation recovery sequences in MR imaging. *J. Comp. Assist. Tomogr.* **9**, 1020–1032.

Bydder, G. M. & Young, I. R. 1985*b* MRI. Clinical use of the inversion recovery sequence. *J. Comp. Assist. Tomogr.* **9**, 659–675.

Chacko, A. K., Szumowski, J., Simon, J. H., Totterman, S., Rubens, D. J., Kyberg, N. S., Kothari, K., Logan-Young, W. W. & Katzberg, R. W. 1989 Comparison of MR sequences, including paramagnetic enhancement actuation by chemical shift imaging (PEACH) in the study of patients presenting with breast pathology of mammography and/or ultrasound. *Proc. 8th A. Mtg Soc. Magn. Reson. Med., Amsterdam*, p. 1065.

Collins, A. G., Bryant, D. J., Young, I. R., Thomas, D. G. T., Gill, S. & Bydder, G. M. 1988 Analysis of the magnitude of susceptibility effects in disease of the brain: implications for NMR spectroscopy. *J. Comp. Assist. Tomogr.* **12**, 775–777.

Cox, I. J., Bryant, D. J., Collins, A. G., George, P., Harman, R. R., Hall, A. S., Hodgson, H. J. F., Khenia, S., McArthur, P. & Spencer, D. H. 1988 Four-dimensional chemical shift imaging of phosphorus metabolites of normal and diseased human liver. *J. Comp. Assist. Tomogr.* **12**, 369–376.

Cox, I. J., Bydder, G. M., Gadian, D. G., Young, I. R., Proctor, E., Williams, S. R. & Hart, I. 1986 The effect of magnetic susceptibility variations in NMR imaging and NMR spectroscopy *in vivo*. *J. magn. Reson.* **70**, 163–168.

De Luca, F., Nuccetelli, C., De Simons, B. C. & Maraviglia, B. 1986 NMR imaging of a solid by the magic-angle rotating-frame method. *J. magn. Reson.* **69**, 496–500.

Dixon, W. T. 1984 Simple proton spectroscopic imaging. *Radiology* **153**, 189–194.

Foster, M. A. 1985 Examining the image slice. *Proc. 2nd A. Cong. Eur. Soc. Magn. Reson. Med. Biol., Montreux*, p. 27.

Garroway, A. N., Grannell, P. K. & Mansfield, P. 1974 Image formation in NMR by a selective irradiative process. *J. Phys.* C **7**, L457–462.

Hahn, E. L. 1959 Spin echoes. *Phys. Rev.* **80**, 580–594.

Hall, A. S., Collins, A. G., Bryant, D. J., Young, I. R. & Bydder, G. M. 1989 Use of solvent suppression resonance technique to enhance changes due to susceptibility variations in magnetic resonance imaging. *Magn. Reson. Med.* **9**, 411–418.

Hore, P. J. 1983 A new method for water suppression in the proton NMR spectra of aqueous solutions. *J. magn. Reson.* **54**, 539–542.

Hoult, D. I. & Chen, C.-N. 1988 The visualisation of probe electric fields reveals intense 'hot-spots'. *Proc. 7th A. Mtg. Soc. Magn. Reson. Med., San Francisco*, p. 892.

Hoult, D. I. & Richards, R. E. 1975 Critical factors in the design of sensitive high resolution nuclear magnetic resonance spectrometers. *Proc. R. Soc. Lond.* A **344**, 311–340.

Hounsfield, G. N. 1973 Computerized transverse axial scanning (tomography). Part 1. Description of system. *Br. J. Radiol.* **46**, 1016–1022.

Hutchison, J. M. S., Edelstein, W. A. & Johnson, E. 1980 A whole body NMR imaging machine. *J. Phys.* E **13**, 947–955.

Koenig, S. H., Brown III, R. D., Gibson, J. F., Ward, R. J. & Peters, T. J. 1986 Relaxometry of ferritin solutions and the influence of the TE3+ core ions. *Magn. Reson. Med.* **3**, 755–767.

Lampman, D., Hivast, G., McNally, J. & Paley, M. 1986 Volume selective ^{1}H NMR spectroscopy with solvent suppression. *Magn. Reson. Imaging* **4**, 115.

PHILOSOPHICAL TRANSACTIONS OF THE ROYAL SOCIETY A MATHEMATICAL, PHYSICAL & ENGINEERING SCIENCES

Laue, E. D., Skilling, J., Staunton, J., Sibisi, S. & Brereton, R. G. 1985 Maximum entropy method in nuclear magnetic resonance spectroscopy. *J. magn. Reson.* **62**, 437–452.

Luyten, P. R., Groen, J. P., Vermeulen, J. W. A. H. & den Hollander, J. A. 1989 Experimental approaches to image localized human ^{31}P spectroscopy. *Magn. Reson. Med.* **11**, 1–21.

Luyten, P. R., Mariën, A. J. H. & den Hollander, J. A. 1988 *In Vivo* ^{1}H NMR spectroscopy of the human brain by spatial localization and imaging techniques. *Proc. 7th A. Mtg, Soc. Magn. Reson. Med., San Francisco*, p. 327.

Naruse, S., Tanaka, C., Higuchi, T., Nishikawa, H., Horikawa, Y. & Ueda, S. 1989 Fully relaxed ^{31}P-MRS of human brain and brain tumors. *Proc. 8th A. Mtg Soc. Magn. Reson. Med., Amsterdam*, p. 76.

National Radiological Protection Board 1983 Revised guidelines on exposure to nuclear resonance clinical imaging. *Br. J. Radiol.* **56**, 974–977.

Nayler, G. L., Firmin, D. N. & Longmore, D. B. 1986 Blood flow imaging by cine magnetic resonance. *J. Comp. Assist. Tomogr.* **10**, 715–722.

Page, D. R., Bryant, D. J. & Young, I. R. 1990 A method for the correction of spectral line shapes. *Proc. 9th A. Mtg, Soc. Magn. Reson. Med., New York*, p. 1094.

Perman, W. H., Bernstein, M. A. & Sandstrom, J. C. 1989 A method for correctly setting the RF flip angle. *Magn. Reson. Med.* **9**, 16–24.

Santyr, G. E., Henkelman, R. M. & Bronskill, M. J. 1989 Spin locking for magnetic resonance imaging with application to human breast. *Magn. Reson. Med.* **12**, 25–37.

Sepponen, R. E., Pohjonen, J. A., Sipponen, J. T. & Tanttu, J. I. 1985 A method for T1ro imaging. *J. Comp. Assist. Tomogr.* **9**, 1007–1011.

Wedeen, V. J., Rosen, B. R., Buxton, R. & Brady, T. J. 1986 Projective MRI angiography and quantitative flow-volume densitometry. *Magn. Reson. Med.* **3**, 226–241.

Weiner, M. W. 1990 Verbal statement, Society of Magnetic Resonance in Medicine/Society of Magnetic Resonance Imaging Joint Symposium, Washington, D.C., 25th February.

Weinmann, H. J., Brasch, H. J., Press, W. R. & Wesbey, G. E. 1984 Characteristics of gadolinium-DTPA complex. A potential NMR contrast agent. *AJR* **142**, 619–624.

Wolff, S. D. & Balaban, R. S. 1989 Magnetization transfer contrast (MTC) and tissue water proton relaxation *in vivo*. *Magn. Reson. Med.* **10**, 135–144.

Young, I. R. 1988 Special pulse sequences and techniques. In *Magnetic resonance imaging* (ed. D. D. Stark & W. G. Bradley), pp. 84–107. St Louis: Mosby.

Young, I. R., Bryant, D. J. & Bydder, G. M. 1989*a* Use of four-dimensional chemical-shift imaging of protons in MR of the brain. *Radiology* **173**, 167.

Young, I. R., Bryant, D. J. & Payne, J. A. 1985 Variations in slice shape and absorption as artefacts in the determination of tissue parameters in NMR imaging. *Magn. Reson. Med.* **2**, 355–389.

Young, I. R., Cox, I. J., Coutts, G. A. & Bydder, G. M. 1989*b* Some considerations concerning susceptibility, longitudinal relaxation time constants and motion artefacts in *in vivo* human spectroscopy. *NMR Biomedicine* **2**, 329–339.

Zhong, J., Gore, J. C. & Armitage, I. H. 1990 T_2 contrast manipulation in MRI by a rotation 'magic angle' RF field. *Magn. Reson. Imaging* **8**, 113.

Discussion

R. D. Farrant (*Wellcome Research Labs, Beckenham, U.K.*). Given the excellent demonstrations of the clinical application of MRI in both assisting diagnosis and monitoring therapy, do we also have a potential tool for possible clinical therapy, particularly of neurological disease?

I. R. Young. In itself MR is unlikely to be useful as a therapy system (e.g. by using its RF sources to deposit energy *in vivo*) though it has been used to observe hyperthermia experiments on line using an additional source and may have a limited

utility in that application. It is more likely to be used in future in therapy in the same way as X-rays are for monitoring interventional procedures on line as suitable catheter-based probes are developed. Whole body MRS has a more immediate potential for monitoring drug response, as demonstrated, for example, by Wolff at UCLA in 1988 at the Radiological Society of North America.

PHILOSOPHICAL TRANSACTIONS OF THE ROYAL SOCIETY A MATHEMATICAL, PHYSICAL & ENGINEERING SCIENCES

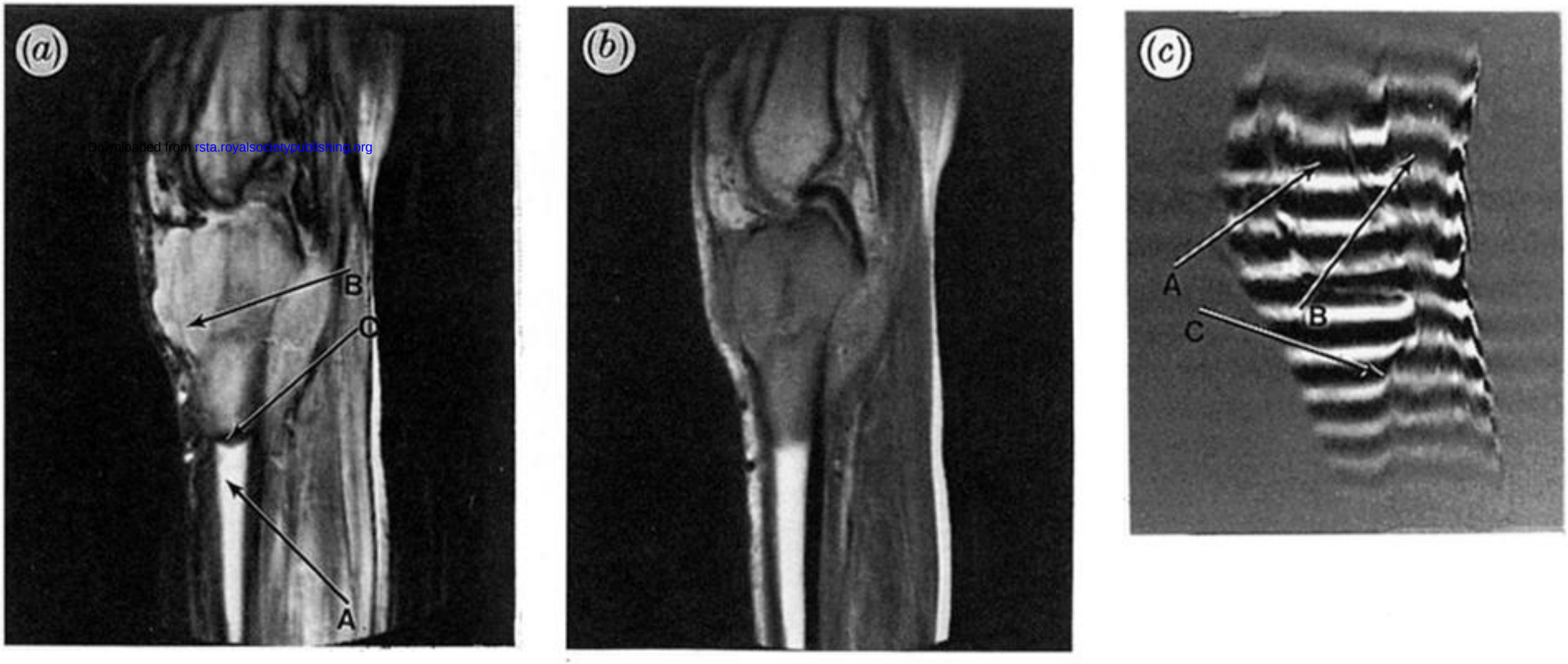

gure 3. Illustration of the manipulation of image contrast and data through the use of methods pendent on the chemical shift difference between water and lipid components of an image. (*a*) agnitude image acquired with T_E chosen to give a phase difference of π between the two mponents ($T_E = 22$ ms, at a field of 0.15 T). The image is of a patient with an osteosarcoma; the agnitude of the signal from the fat components in the bone marrow (arrow A) is similar to that om the tumour (arrow B). The line (arrow C) between the two is the place where the signals from e two overlap in the same voxels, and cancel, because they are out of phase, so that a minimum observed. (*b*) Hahn spin echo of the same patient, with no dephasing between the lipid and water mponents, and, consequently, loss of the delineating line seen in figure 3*a*. (*c*) 'Zebra stripe' nage of the leg of a volunteer in which a phase difference imposed by the phase correction of one nage by another (see main text) results in a phase pattern, which is shifted between the lipid and ater components (arrows A, B). The image also shows the characteristic distortion of phase lines ue to moving spins (in the blood vessels, for example) (arrow C, and see main text).

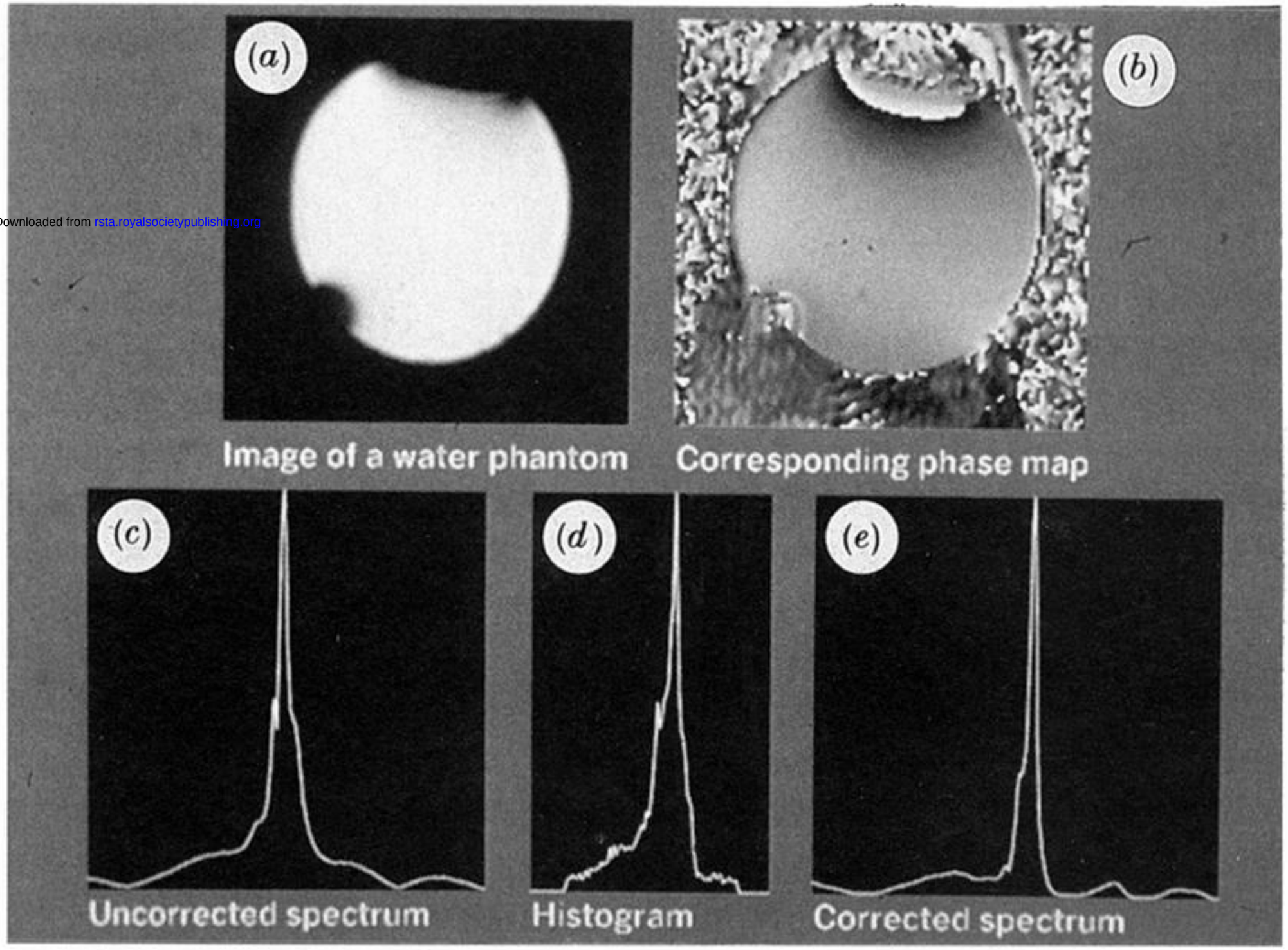

gure 7. Illustration of the similarity between the line shape of a simple spectrum and histograms rmed from the voxel field deviations as observed through field mapping, and the use of the latter r line-shape correction. (*a*), (*b*) Magnitude image and phase map of a plane from which one ectrum in a one-dimensional phase encoding ^{1}H spectroscopic experiment is to be recovered. (*c*) pectrum extracted from the plane in (*a*). (*d*) Histogram of the field deviations mapped in image). Note the similarity of the shape of (*c*) and (*d*), though the former should be a lorentzian. (*e*) rrected spectrum formed as described in the text.

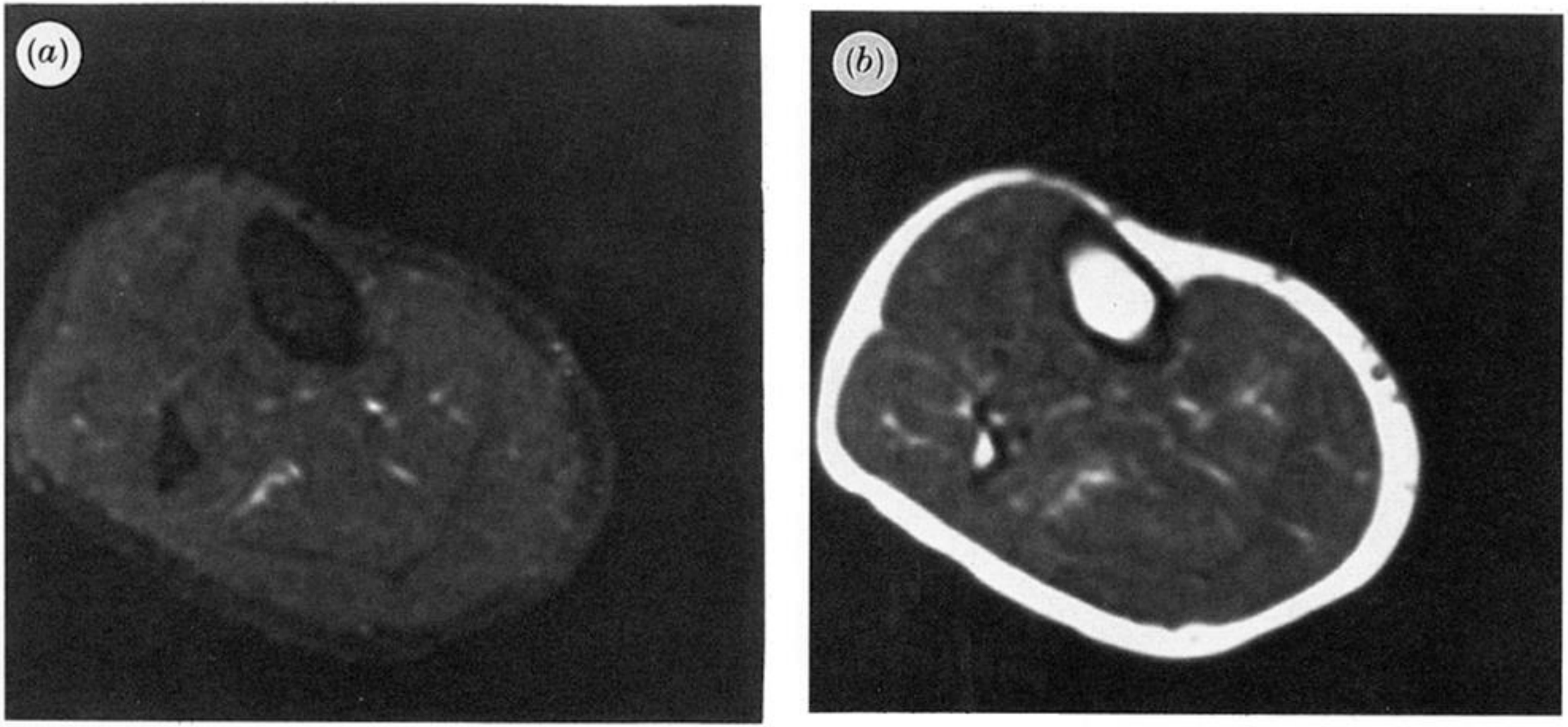

gure 10. Images to illustrate the use of the selective excitation method described. Both images ave a matrix of 128×128; slice thickness of 10 mm; resolution of 1.5 mm^2, and sequence petition time 1500 ms. (*a*) Normal spin echo. (*b*) Image in which only the water line has been cited.

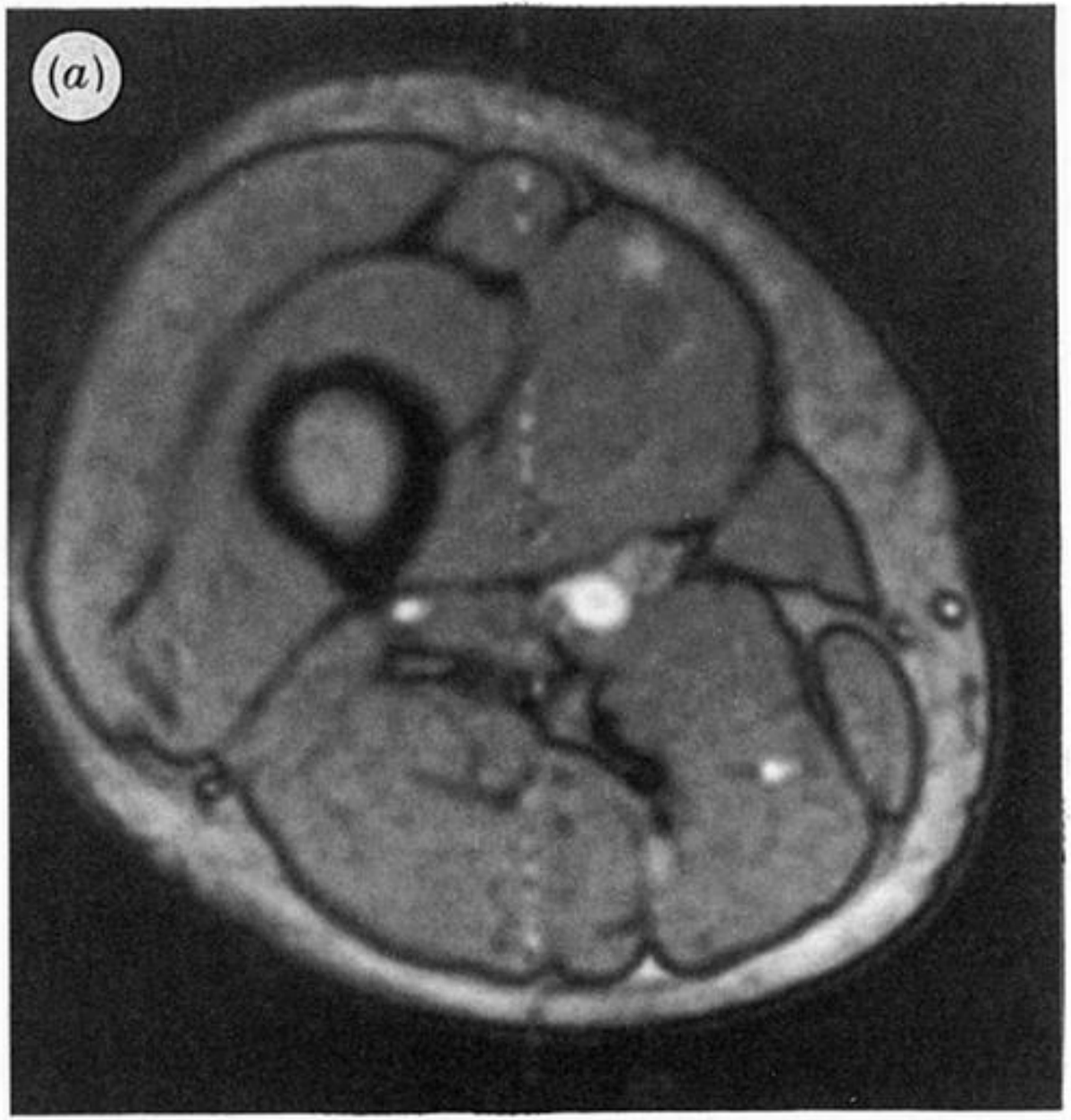

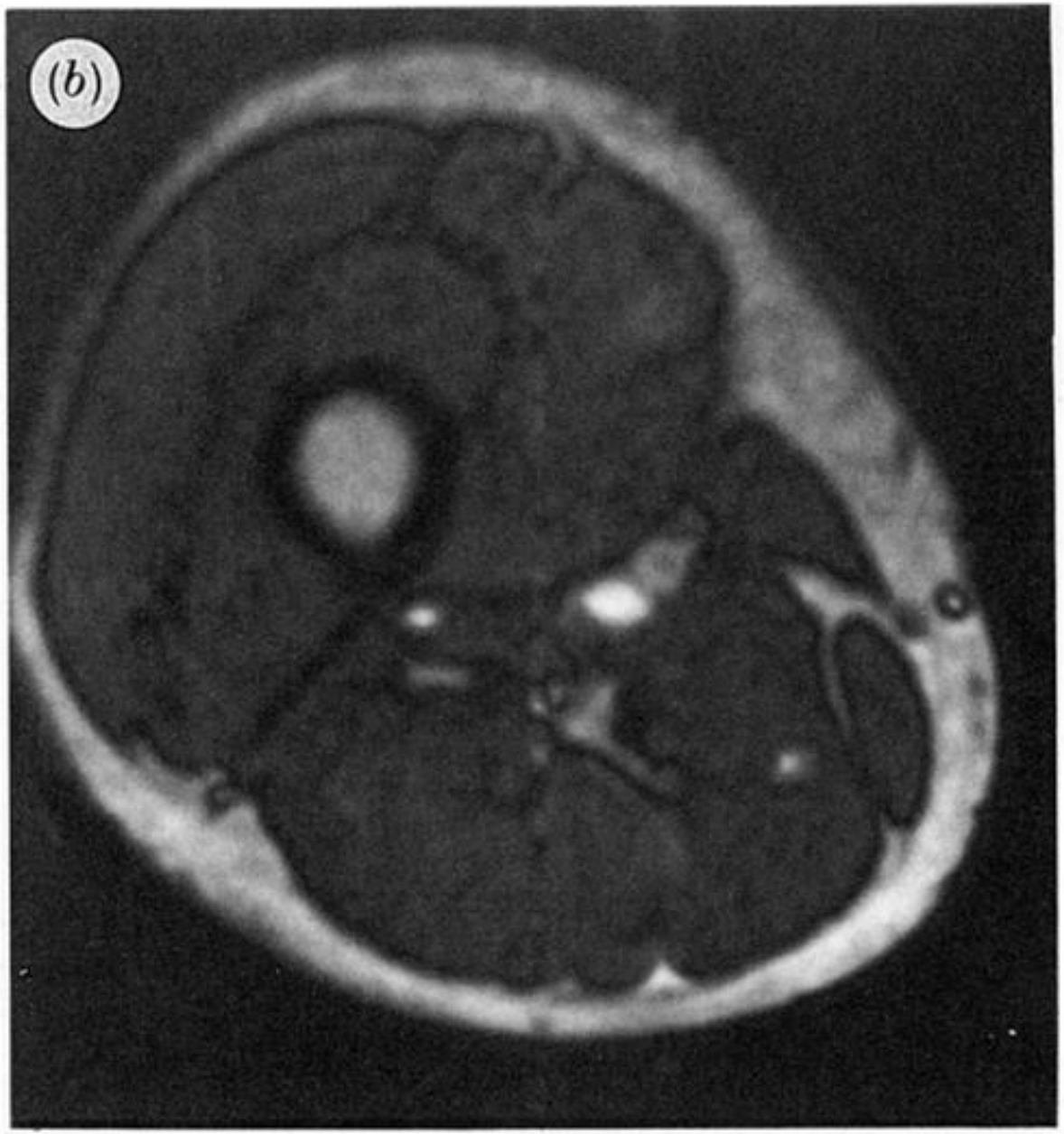

gure 11. Pair of images obtained with $T_R = 1000$ ms, $T_E = 44$ ms; matrix 128×128; resolution 5×1.5 mm; slice thickness 10 mm. (*a*) Normal spin echo. (*b*) Same acquisition as above except th 100 ms RF pre-pulse of 27 μT irradiation at an offset frequency of 2 kHz from resonance.